Review of Scientific Instruments

In situ measurement equipment for the elastic wave velocity of rocks under various temperature and pressure conditions of ultra-deep reservoirs

Cite as: Rev. Sci. Instrum. **93**, 114502 (2022); https://doi.org/10.1063/5.0099911
Submitted: 19 May 2022 • Accepted: 19 October 2022 • Published Online: 14 November 2022

Shuai Wang, Heping Li, Yonggang Liu, et al.

AIP Publishing

Review of Scientific Instruments ARTICLE scitation.org/journal/rsi

In situ measurement equipment for the elastic wave velocity of rocks under various temperature and pressure conditions of ultra-deep reservoirs

Cite as: Rev. Sci. Instrum. 93, 114502 (2022); doi: 10.1063/5.0099911
Submitted: 19 May 2022 • Accepted: 19 October 2022 •
Published Online: 14 November 2022

Shuai Wang,[1,2] Heping Li,[1,a)] Yonggang Liu,[1,a)] Shengbin Li,[1] Shuangming Shan,[1] and Sen Lin[1]

AFFILIATIONS

[1] Key Laboratory of High-Temperature and High-Pressure Study of the Earth's Interior, Institute of Geochemistry, Chinese Academy of Sciences, Guiyang 550081, China
[2] University of Chinese Academy of Sciences, Beijing 100049, China

[a)] **Authors to whom correspondence should be addressed:** liheping@mail.gyig.ac.cn and liuyonggang@vip.gyig.ac.cn

ABSTRACT

A novel equipment for measuring the elastic wave velocity of rocks under various temperature and pressure conditions of ultra-deep reservoirs has been developed. The equipment consists of a high pressure and high temperature experimental platform and an ultrasonic measurement system, which can measure the elastic wave velocity of rocks under conditions of ultra-deep reservoirs up to a depth of 13 km by the ultrasonic reflection method. The method of assembling rock samples has also been improved to acquire high-quality ultrasonic signals. The feasibility of the new equipment was tested by measuring the elastic wave velocity of dolomite and limestone. The experimental results are consistent with the previous research. The elastic wave velocity of rocks measured by this equipment can be potentially used for the exploration of ultra-deep oil and gas resources.

I. INTRODUCTION

The elastic wave velocity of ultra-deep reservoir rocks usually refers to the propagation velocity of ultrasonic[1,2] or seismic waves[3] through rocks in reservoirs deeper than 6 km.[4] It plays an extremely important role in reservoir exploration,[5,6] which can explain the structure of seismic wave velocity[7] and constrain the uncertainty in geophysics inversion.[8,9] Therefore, the elastic wave velocity of ultra-deep reservoir rocks has become an indispensable parameter in the process of oil and gas resources exploration.[10–13]

Based on its importance, some devices that can simulate temperature and pressure conditions of ultra-deep reservoirs and simultaneously allow measurement of rock elastic wave velocity have been developed.[14] Notably, the devices in this paper mainly refer to the autoclave[15] and autoclave-like pressure vessel, rather than the multi-anvil large volume press,[16–18] diamond anvil cell,[19] and piston cylinder press,[20] which are commonly used in the field of high-pressure science. This is because the temperature and pressure values of the autoclave are more accurate than the other three in the temperature and pressure range of the Earth's crust.[21] Therefore, the autoclave is probably the most suitable device for simulating the conditions of the ultra-deep reservoirs among the existing high-pressure devices.[22]

In the following text, some of such devices as stated above and related experimental reports are listed. Kitamura *et al.*[23] developed a new device for measuring the elastic wave velocity of rocks under the *in situ* conditions of the crust, which are characterized by high pressure (up to 200 MPa), high temperature (up to 200 °C), and the existence of pore fluids. Watanabe *et al.*[24] designed a device for measuring the elastic wave velocity of fluid-saturated rocks at various confining and pore-fluid pressures. The confining pressure of the device can reach up to 200 MPa, using silicone oil as the pressure transfer medium. Zappone *et al.*[25] measured the elastic wave velocity of rocks at room temperature and pressure of up to 280 MPa with the help of a pressure vessel in the Laboratory of Petrophysics at Milano. Li *et al.*[26] measured the elastic wave velocity of

bitumen-saturated sandstone by a high-pressure vessel with the maximum temperature of 200 °C and the maximum confining pressure of 50 MPa.

To the best of our knowledge, in addition to the above-stated autoclave and pressure vessel used in laboratories, a number of commercially available devices compatible with measuring elastic wave velocity of rocks under conditions of deep and ultra-deep reservoirs have been developed by several companies, some of which are listed in Table I.

As shown in Table I, the limit values of some commercially available device parameters are listed. The following text is a relatively rough calculation for the maximum depth of reservoirs that can be simulated by the devices in Table I. The ground temperature is assumed to be 15 °C and the average geothermal gradient is 3 °C/100 m.[31] The formula for calculating the lithostatic pressure is $p = \rho gh$,[32] where ρ is taken as the average crustal density of 2.7 g/cm^3.[33] If the corresponding depth of reservoirs is calculated according to the geothermal gradient and lithostatic pressure stated above, as shown in Table I, there are very few devices that can measure the elastic wave velocity of rocks under reservoir conditions equivalent to a depth of 8 km. The reasons for the limitations in the temperature and pressure of these devices mainly include the use of silicone oil as the pressure transmission medium,[24,26] which cannot be used at temperatures higher than about 300 °C,[34] and the materials used in these devices to seal rock samples, such as rubber, cannot withstand high temperatures.[35–37]

However, with the massive exploitation and consumption of shallow crustal energy and mineral resources, many countries have extended natural resource exploration areas and target layers from the intermediate and shallow layer to the deep and ultra-deep layer.[38] Globally, 120 ultra-deep oil and gas fields have been found in six basins with the most abundant ultra-deep oil and gas reservoirs, including the Mexican Bay Basin (USA), the Tarim Basin (China), etc.,[39] among which the deepest drilling in China's Tarim Basin has reached 8882 m.[40] Nevertheless, as stated above, very few devices currently available for measuring the elastic wave velocity of rocks can reach the temperature and pressure conditions equivalent to a depth of 8 km, which seriously hinders the development of ultra-deep reservoir exploration.[41] Therefore, there is an urgent need to develop a new device that can measure the elastic wave velocity of rocks under the conditions of reservoirs deeper than 8 km.

In order to meet the above needs, an *in situ* measurement equipment for the elastic wave velocity of rocks under temperature and pressure conditions of ultra-deep reservoirs up to a depth of 13 km has been developed on the high pressures and high temperatures (HPHT) experimental platform of the Key Laboratory of High-Temperature and High-Pressure Study of the Earth's Interior, Chinese Academy of Sciences. The HPHT experimental platform is compatible with measuring multiple physical properties of rocks. Electrical conductivity and porosity of rocks have been successfully measured on this platform previously.[22,42] Our aim is to introduce an ultrasonic measurement system on this platform to make it capable of measuring elastic wave velocities of rocks in conditions of ultra-deep reservoirs up to 13 km deep. In the following, the paper will describe in detail the components and measurement principles of the equipment, the validation of the experimental results, and the potential applications of the equipment.

II. EQUIPMENT AND MEASUREMENT PRINCIPLE

The *in situ* measurement equipment for the elastic wave velocity of rocks under temperature and pressure conditions of an ultra-deep reservoir mainly includes the HPHT experimental platform and the ultrasonic measurement system, in which the former is mainly used to simulate the conditions of ultra-deep reservoirs and the latter serves to measure the wave velocity of rocks. The combination and compatibility of these two systems and the acquisition of clean and clear ultrasonic signals of rock samples under HPHT conditions are the focus of the whole work.

A. HPHT experimental platform

The HPHT experimental platform, which is mainly consisted of the resistance furnace (Shanghai Y-feng Electrical Furnace Co., Ltd., YFFKH130X650/10T), temperature controller (Xiamen Yudian Automation Technology Co., Ltd., AI-808P), gas pressurizing device,[43] and autoclave,[44] can simulate the temperature and pressure conditions of reservoirs up to a depth of 13 km. As shown in Fig. 1(a), the autoclave is placed in the resistance furnace. The resistance furnace heats the autoclave from the outside and the maximum heating temperature of the resistance furnace can be up to 1000 °C. The temperature in the resistance furnace is controlled by the temperature controller, and the precision of temperature control is ±2 °C. The gas pressurizing device uses argon gas,[23] which can withstand high temperatures, as the pressure transmission medium. The maximum hydrostatic pressure that can be achieved is 400 MPa, with an uncertainty of ±2 MPa.[43] As the vital part of the

TABLE I. Parameters of commercially available devices for measuring the elastic wave velocity of rocks under conditions of reservoirs.

Company	Devices	Limit values of devices parameters		Simulated depth (km)
		Temp. (°C)	Confining P (MPa)	
MTS[27]	Series 656 triaxial cells	200	140	5.2
NER[28]	High temperature AutoLab	300	200	7.4
GCTS[29]	RTR series	200	210	6.1
WILLE Geotechnik[30]	HPHT triaxial system	250	210	7.8

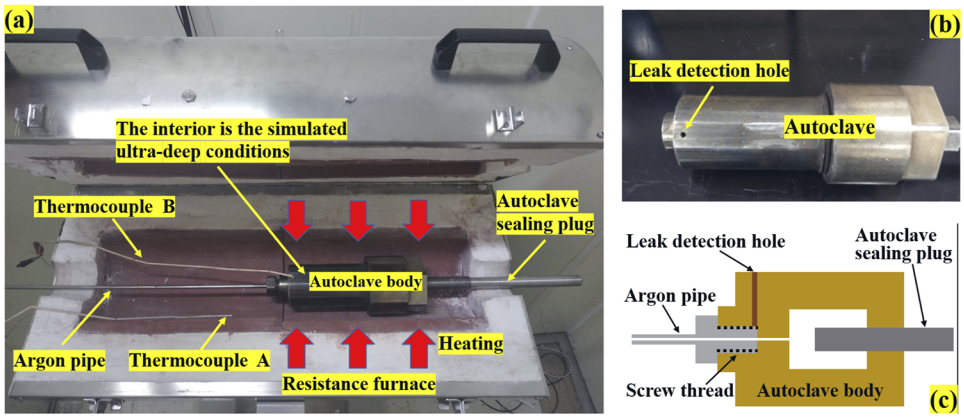

FIG. 1. (a) Image of the HPHT experimental platform. The temperature controller and gas pressurizing device are located at the experimental control room next to the resistance furnace. (b) The leak detection hole of the autoclave. (c) Sectional view of the leak detection hole of the autoclave.

HPHT experimental platform, the autoclave consists of an autoclave body and an autoclave sealing plug, which can strictly seal the high-pressure argon gas of 350 MPa.[22] Moreover, it is worth noting that, as shown in Fig. 1(a), due to the temperature gradient along the wall thickness of the autoclave, two NiCr–NiSi thermocouples are required during the experiment, where thermocouple A is connected to the temperature controller and thermocouple B is connected to a separate thermometer. During the experiment, thermocouple A was placed in the outside of the autoclave to measure the actual temperature in the resistance furnace, while thermocouple B, as shown in Fig. 1, was placed in the leak detection hole leading to the deep part of the autoclave body to measure the temperature in the autoclave. Since the temperature in the autoclave was measured by placing thermocouple B in the leak detection hole during the experiment, instead of directly measuring the temperature in the autoclave, some error theoretically exists in this type of temperature measurement, for which we will specify the magnitude of this error later in the paper. Finally, the working principle of the HPHT experimental platform is shown in Fig. 1(a). When the autoclave is filled with high-pressure argon and simultaneously externally heated, a high temperature and high hydrostatic pressure condition can be formed in the autoclave to simulate the conditions of the ultra-deep reservoir.

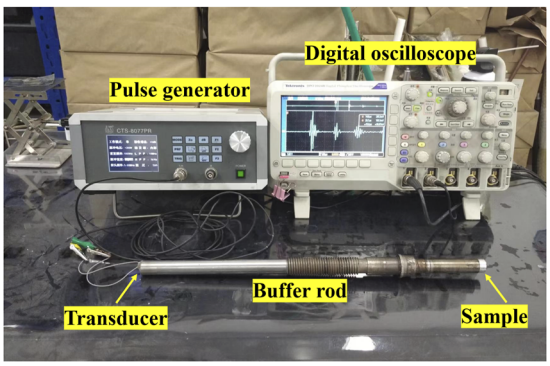

FIG. 2. The physical picture of the ultrasonic measurement system.

B. The ultrasonic measurement system

It can be found from Fig. 2 that the ultrasonic measurement system is mainly consisted of a pulse generator (Guang-dong Goworld Co., Ltd., CTS-8077PR), digital oscilloscope (Tektronix DPO2024B), dual-mode ultrasonic transducer, and buffer rod. The electrical pulse generated by the pulse generator excites the transducer to generate ultrasonic waves. The ultrasonic waves pass through the buffer rod and the rock sample in turn and are reflected at the two ends of the rock samples. The pulse generator receives the reflected signals and then sends them to the digital oscilloscope for display and storage. Specifically, the two ends of the buffer rod are flat and smooth, with one end in contact with the rock sample and the other end glued with the ultrasonic transducer by epoxy glue (Henkel Pattex AB glue). The dual-mode ultrasonic transducer used in the experiments is a homemade transducer that we made from easily available lead zirconate titanate (PZT) piezoceramic materials based on the existing technology.[45] The dual-mode ultrasonic transducer during the experiment can generate compression waves of 5 MHz and shear waves of 2.5 MHz simultaneously. The highest data acquisition rate of the digital oscilloscope is 1 G/s, and the corresponding time resolution of the acquired data is 1 ns.

C. The combination of HPHT experimental platform and ultrasonic measurement system

In order to make the HPHT experimental platform compatible with the ultrasonic measurement system, there are six main challenges needed to be solved, including the improvement of the autoclave sealing plug, the cooling of the transducer and the feasibility verification of the cooling method, the large temperature gradient along the wall thickness of the autoclave, the check of whether the rock is in the far field, the sealing of the rock sample, and the design of the suitable rock thickness. In the following text, we will elaborate on the solutions to the challenges stated above.

As stated above, the autoclave consists of an autoclave body and an autoclave sealing plug. The close contact between the sealing plug and the autoclave body enables the autoclave to strictly seal high-pressure gas. The sealing principle of the autoclave was detailed in a patent.[44] As shown in Fig. 1(a), the autoclave sealing plug is a regular cylindrical rod. One end of the autoclave sealing plug was exposed to the simulated ultra-deep reservoir conditions inside the

autoclave and the other end was exposed to the normal temperature and pressure conditions outside the autoclave. Obviously, as shown in Figs. 1(a) and 2, the autoclave sealing plug can also be used as an ultrasonic buffer rod to realize the combination of the HPHT experimental platform and the ultrasonic measurement system. For the purpose of making the autoclave sealing plug more suitable as an ultrasonic buffer rod, we have made two improvements to the sealing plug. First, in order to meet the requirements for the low ultrasonic attenuation of the buffer rod and the high strength of the sealing material at the same time, the material of the autoclave sealing plug was changed from Titanium alloy to stainless steel. Second, as shown in Fig. 1(a), when the resistance furnace heats the autoclave body, it also heats the sealing plug and the transducer. The high temperature will affect the transducer[46] and the epoxy adhesive,[47] which will deteriorate the ultrasonic measurements. To solve this problem, we used a circulating coolant (water) at the tail of the buffer rod and extended the length of the buffer rod to 42, 17 cm of which is outside of the resistance furnace and the rest is inside of the resistance furnace.

Obviously, the temperature at the transducer needs to be measured to verify the efficiency of the coolant and the temperature at the end face of the buffer rod also needs to be measured to verify whether the temperature gradient in the axial direction of the buffer rod, caused by the coolant at the end of the buffer rod and the high temperature of the resistance furnace, affects the rock temperature. In addition, as stated above, the thermocouple was placed in the leak detection hole of the autoclave body during the experiment, instead of directly measuring the temperature in the autoclave, which would bring some error to the measurement of the rock temperature. In order to clarify the magnitude of the error, the temperature in the leak detection hole and the temperature in the autoclave also need to be measured. As shown in Fig. 3(a), the temperature at the transducer, the temperature at the end of the buffer rod, the temperature in the autoclave, and the temperature in the leak detection hole were measured by thermocouples 1, 2, 3, and 4 under atmospheric pressure conditions. In addition, thermocouple 5, which is connected to the temperature controller controlling the temperature of the resistance furnace, is used to measure the temperature in the resistance furnace. The experiment was conducted by increasing the temperature in the resistance furnace to 450 °C at a heating rate of 100 °C/h. When the temperature measured by thermocouple 3 was room temperature, 100, 200, 300, 350, and 400 °C, respectively, the temperature measured by several other thermocouples was recorded. The measurement results are shown in Fig. 3(b), where the horizontal coordinate is the temperature measured by thermocouple 3. As can be seen in Fig. 3(b), the coolant can keep the temperature of the transducer at room temperature during the experiment due to its fast flow. The temperatures measured by thermocouple 3 and thermocouple 2 are basically the same, which means that the temperature gradient in the axial direction of the buffer rod has almost no effect on the rock temperature due to the sufficiently long length of the buffer rod. Although the temperature measured by thermocouple 4 should theoretically be somewhat higher than the temperature measured by thermocouple 3, they were basically the same during the experiment, with the difference of no more than 1 °C, which indicates that the temperature in the leak detection hole can be considered as the temperature in the autoclave. That is, the temperature of the rock in the autoclave can be measured by placing the thermocouple in the leak detection hole during the experiment.

Furthermore, it is obvious from Fig. 3(b) that there is a large temperature gradient along the wall thickness of the autoclave. In order to further investigate the magnitude of the temperature gradient during the heating process, the following detailed experiments were conducted. The experimental procedure was as follows: the temperature in the resistance furnace was heated to 100 °C at a heating rate of 100 °C/h and then the temperature was kept constant. The temperatures inside and outside of the autoclave were measured by the thermocouple 3 and 5 in Fig. 3(a), respectively. The experimental results are shown in Fig. 4. As can be seen from Fig. 4, due to the thick wall of the autoclave, the temperature difference between the inside and outside of the autoclave is still about 10 °C after 5 h of maintaining the temperature in the resistance furnace, and as the temperature difference between the resistance furnace and the inside of the autoclave decreases, the heating rate inside the autoclave, which is only determined by the temperature

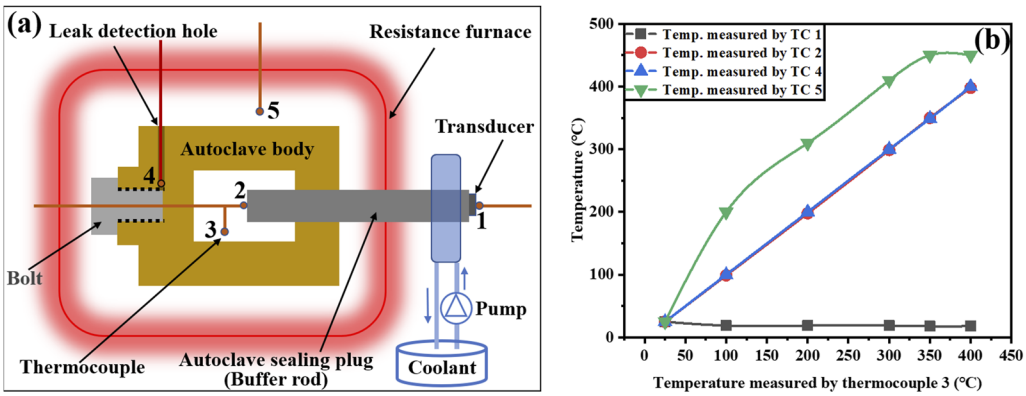

FIG. 3. (a) Temperature measurement by thermocouples 1, 2, 3, 4, and 5. (b) Comparison of the temperature measured by thermocouple 3 and the temperature measured by thermocouples 1, 2, 4, and 5. TC is the abbreviation for the thermocouple.

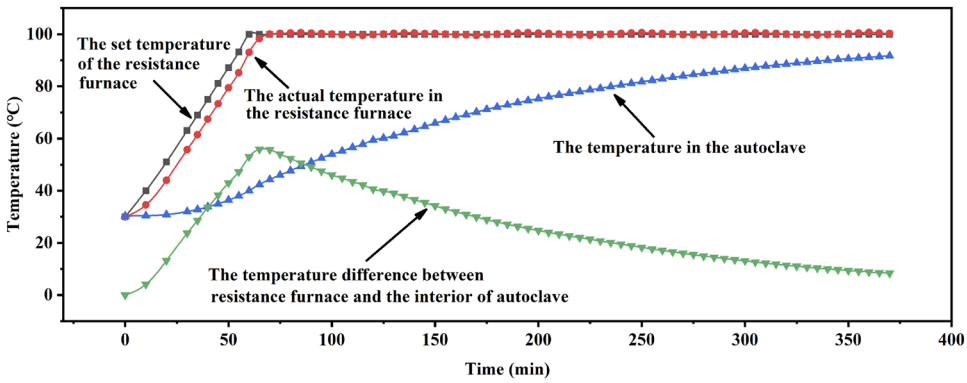

FIG. 4. The temperature difference between the resistance furnace and the autoclave.

difference, also decreases, so it needs a lot of time for the temperature in the autoclave to reach the target temperature. Therefore, raising the temperature in the autoclave to the target temperature in a relatively short period of time may be a potential challenge that needs to be solved, especially in practical applications where multiple rock samples need to be measured with this equipment as well as elastic wave velocities of rocks need to be measured at multiple temperature conditions. In order to counteract the potential problem, the holding temperature of the resistance furnace can be set slightly higher than the target temperature of the autoclave. As shown in Fig. 4, the heating rate inside the autoclave at the temperature difference of 25 °C is already slow, usually 1.5 °C/10 min, and 10 min is enough to complete the measurement of the rock elastic wave velocity at different pressures on this equipment. Moreover, both the space inside the autoclave and the volume of the rock used in the experiment are small, with the rock volume being only about 1.8 cm^3, so it can be assumed that the temperature of the rock is uniform during the measurement of the rock elastic wave velocity. Therefore, during the heating of the autoclave to reach the target temperature, the autoclave can be kept at a temperature no higher than the target temperature of 25 °C to allow the temperature in the autoclave to reach the target temperature in a relatively short period of time.

In addition, since the length of the buffer rod, which was also the distance of the rock sample from the transducer, has been determined after the above verification, a check could be made to determine whether the rock was in the far field. According to the previous paper,[48] it is known that whether the sample is in the far field can be determined from the relationship between $2D^2/\lambda$ and r, where D is the radius of the transducer, λ is the wavelength, and r is the distance of the rock from the transducer. According to the parameters of this experiment, D of 4 mm, λ of about 1.4 mm, and r of 42 cm, it is known that $r \gg 2D^2/\lambda$ of this experiment, so the rock is in the far field.

The fifth challenge is that how to seal the rock samples under high temperature and high hydrostatic pressure conditions. After many failures, as shown in Fig. 5, the welding method was used to seal the rock samples. The open end of the sealing tube made of copper is soldered with the buffer rod. The wall thickness of the sealing tube body is about 0.2 mm, which is thin enough without affecting the transmission of the confining pressure. In addition, in order to solve the problem that the method of ultrasonic reflection is not suitable for natural rocks due to the severe ultrasonic attenuation of rocks,[49] we used tungsten carbide (WC) blocks as a reflector. The acoustic impedance mismatch between the rock and WC can enhance the reflected signal from the end face of the rock.[50]

The next challenge is that since the buffer rod also takes on the function of sealing, there is a section of the protruding structure with sealing effect at the head of the buffer rod as shown in Fig. 5(a), which caused some unwanted clutter in the time-domain signal. In order to avoid the overlap of the clutter with the target signals, it is necessary to design a suitable thickness of the rock sample. Figure 6(a) is the time-domain signal when the rock sample is not mounted, where waveform A1 is the reflected signal from the end face of the buffer rod, and waveform A_3 and the waveforms following it are unwanted clutter. Therefore, if the overlap between the rock signal and the clutter signals is to be avoided, the rock signal

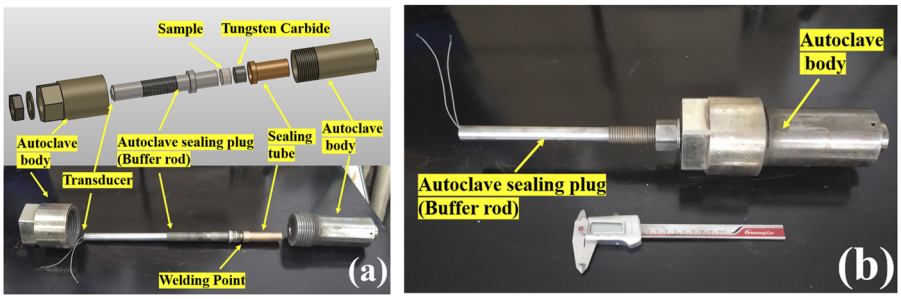

FIG. 5. (a) The autoclave sealing plug acts as a buffer rod. (b) Assembled autoclave.

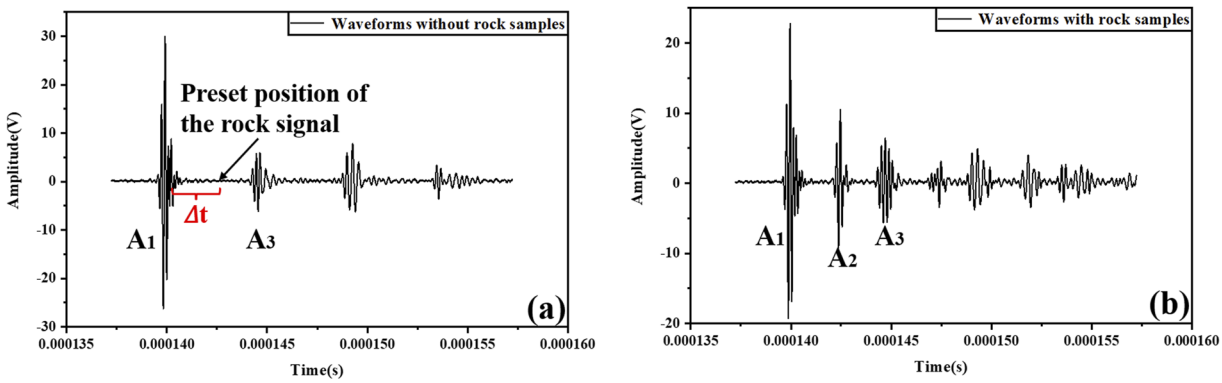

FIG. 6. (a) Time-domain signal without rock samples. (b) Time-domain signal with the rock sample.

should preferably appear in the middle of waveforms A_1 and A_3, that is, the travel time of ultrasonic waves in the rock sample is roughly Δt in Fig. 6(a). In order to make the rock signal appear at the position stated above, a design for a suitable rock thickness L needs to be made based on the approximate wave velocity of rocks and the preset ultrasonic travel time Δt in the rock. Therefore, first, the elastic wave velocity v of the rock is measured under normal temperature and pressure conditions, and then the desired rock thickness L can be obtained according to the equation $(v \cdot \Delta t)/2 = L$. Figure 6(b) shows the time-domain signal when a rock sample coupled by vaseline is measured, where waveform A_2 is the desired rock signal that appears at the preset position.

Finally, the schematic diagram of the whole equipment is shown in Fig. 7. Its specific working principle is as follows. By heating and pressurizing the autoclave, the rock sample sealed by the tube in the autoclave will be in simulated HPHT conditions. The pulse generator sends electric pulses to the ultrasonic transducer, which can convert the electrical pulses into ultrasonic waves. The ultrasonic waves successively pass through the buffer rod, rock sample, and WC. Correspondingly, the reflected ultrasonic signals at each interface will be received by the transducer and finally recorded by a digital oscilloscope. As shown in Fig. 7, waveforms A_1 and A_2 are the reflected signals at interfaces a and b, respectively, and the other waveforms can be considered as clutter because they are not involved in the calculation of the elastic wave velocity of rocks. According to the inverse phase relationship between waveforms A_1 and A_2, the peak of waveform A_1 and the corresponding trough of A_2 in Fig. 7 are read, whose travel times are recorded as T_1 and T_2, respectively. T_1 and T_2 are the crucial data of our experiments to derive the ultrasonic velocity of rock samples. According to the work of Liu *et al.*,[7,49] the elastic wave velocity of rocks can be calculated according to Eq. (1), in which L is the rock thickness,

$$V = 2L/(T_2 - T_1). \tag{1}$$

III. TESTING

A. Rock samples and experimental process

The natural rock samples of limestone and dolomite used in the experiment are collected from Hanyuan, Sichuan, China. The

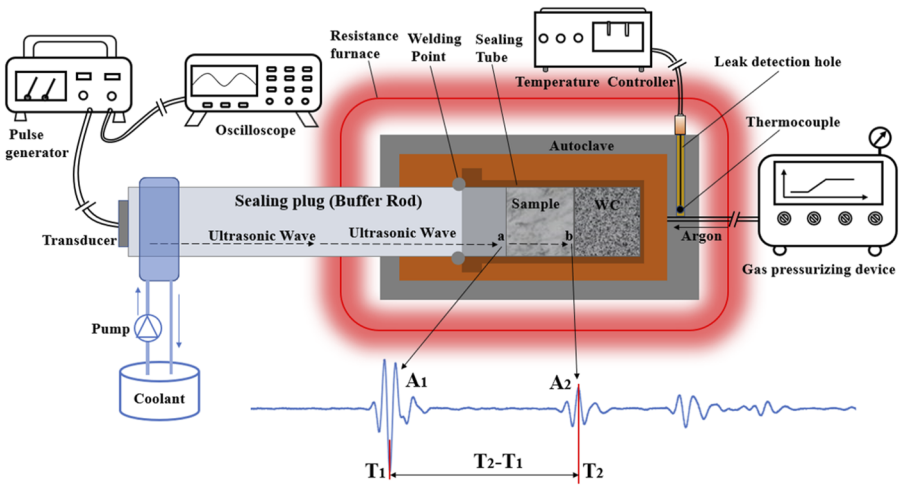

FIG. 7. Schematic diagram of the equipment and measuring principle.

TABLE II. Physical parameters of rock samples.

Rock samples	Sampling location			Rock sample size (mm)		Density (g/cm^3)
	Longitude	Latitude	Altitude (m)	Diameter	Length	
Dolomite	N 29° 20′ 41″	E 103° 05′ 26″	982	18.00	7.05	2.86
Limestone	N 29° 01′ 36″	E 102° 48′ 11″	1060	18.00	7.70	2.83

specific parameters of rock samples are listed in Table II. These samples were processed into cylinders with a diameter of 18 mm. The two end faces of the samples were polished to be smooth, parallel to each other and perpendicular to the central axis. The thickness and diameter of samples were measured by vernier calipers with an accuracy of 0.01 mm. The measured thickness is denoted as L, which is used to calculate the elastic wave velocity of rocks in Eq. (1). Before the measurements, the samples are dried to a constant weight at the temperature of 100 °C for 12 h to prevent pore water from affecting the elastic wave velocity.

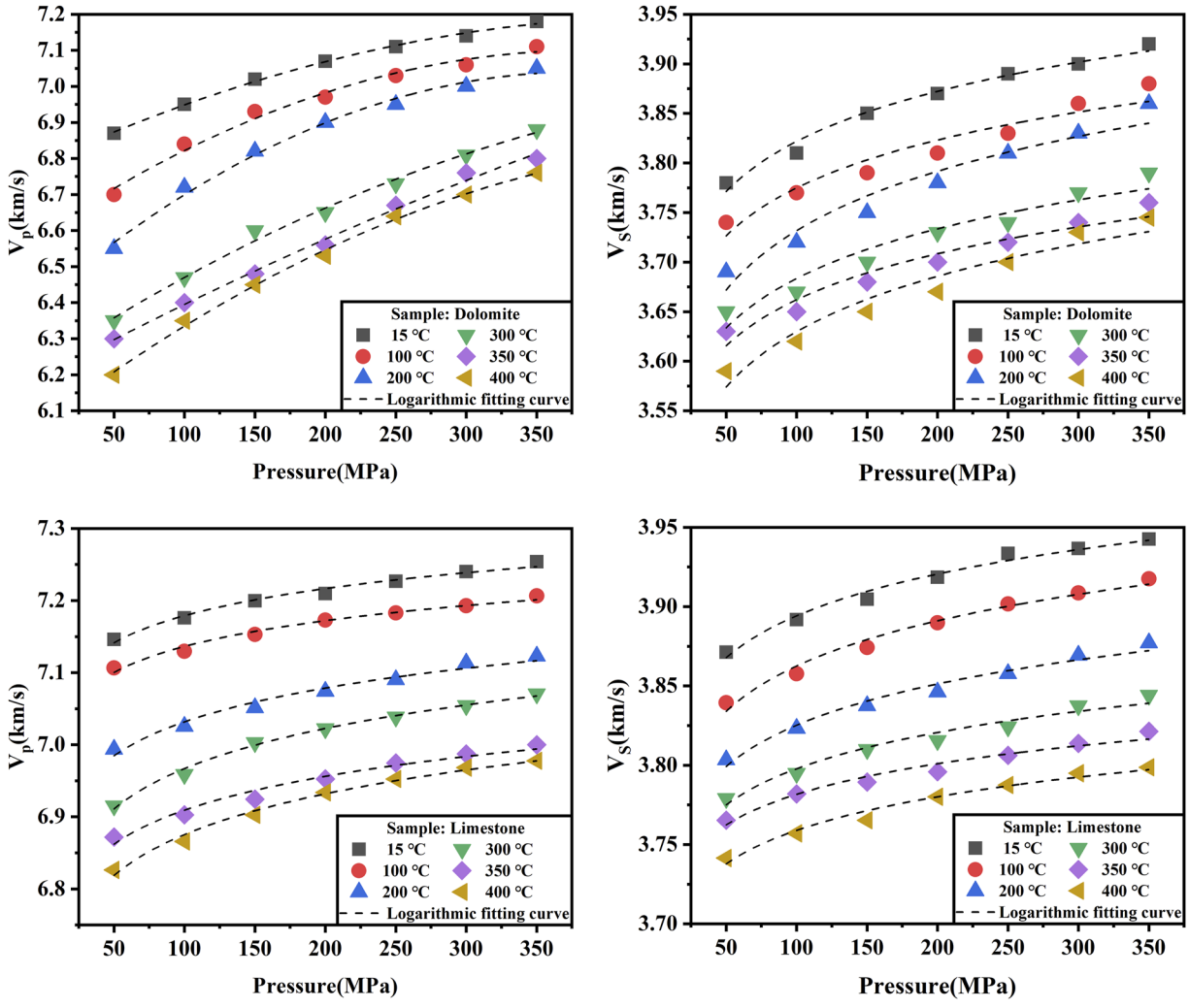

FIG. 8. The relationship between V_P and V_S of dolomite and limestone with pressure.

Measurements were carried out under high pressure conditions up to 350 MPa and high temperature conditions up to 400 °C. Compression and shear wave velocities (V_P and V_S) of rock samples were recorded at about 50 MPa intervals for increasing pressure and at six levels of temperature, including 20 °C (room temperature), 100, 200, 300, 350, and 400 °C. Notably, these temperatures refer to the temperature in the autoclave, instead of the temperature in the resistance furnace. Based on the measurement of the temperature gradient and the analysis of the heating rate inside the autoclave in Sec. II, the holding temperature of the resistance furnace was set to 45, 125, 225, 325, 375, and 425 °C, which were 25 °C higher than the target temperature, respectively. In the experiment, after the resistance furnace reaches a set temperature at a heating rate of 100 °C/h, the temperature in the resistance furnace is kept constant, and the temperature in the autoclave is increased by the temperature difference between the resistance furnace and the inside of the autoclave. When the temperature in the autoclave rises to the target temperature, the elastic wave velocities of the rocks are measured sequentially at different confining pressures from atmospheric pressure to 350 MPa in steps of 50 MPa.

In addition, some other important parameters related to the experiment are as follows. The frequencies of compression and shear waves are 5 and 2.5 MHz, respectively. The output of the pulse generator in the experiment is square wave pulses with the pulse voltage of −200 V, the repetition frequency of 1000 Hz, and the pulse width of 100 ns for compression wave and 200 ns for shear wave. The data acquisition rate of the digital oscilloscope in the experiment is 1 G/s, and the time resolution of the acquired data is 1 ns.

B. Experimental results

1. The effect of pressure on elastic wave velocity of limestone and dolomite

The experimental results for the effect of pressure on the elastic wave velocity of limestone and dolomite are shown in Fig. 8. When the temperature is constant, both the V_P and V_S of limestone and

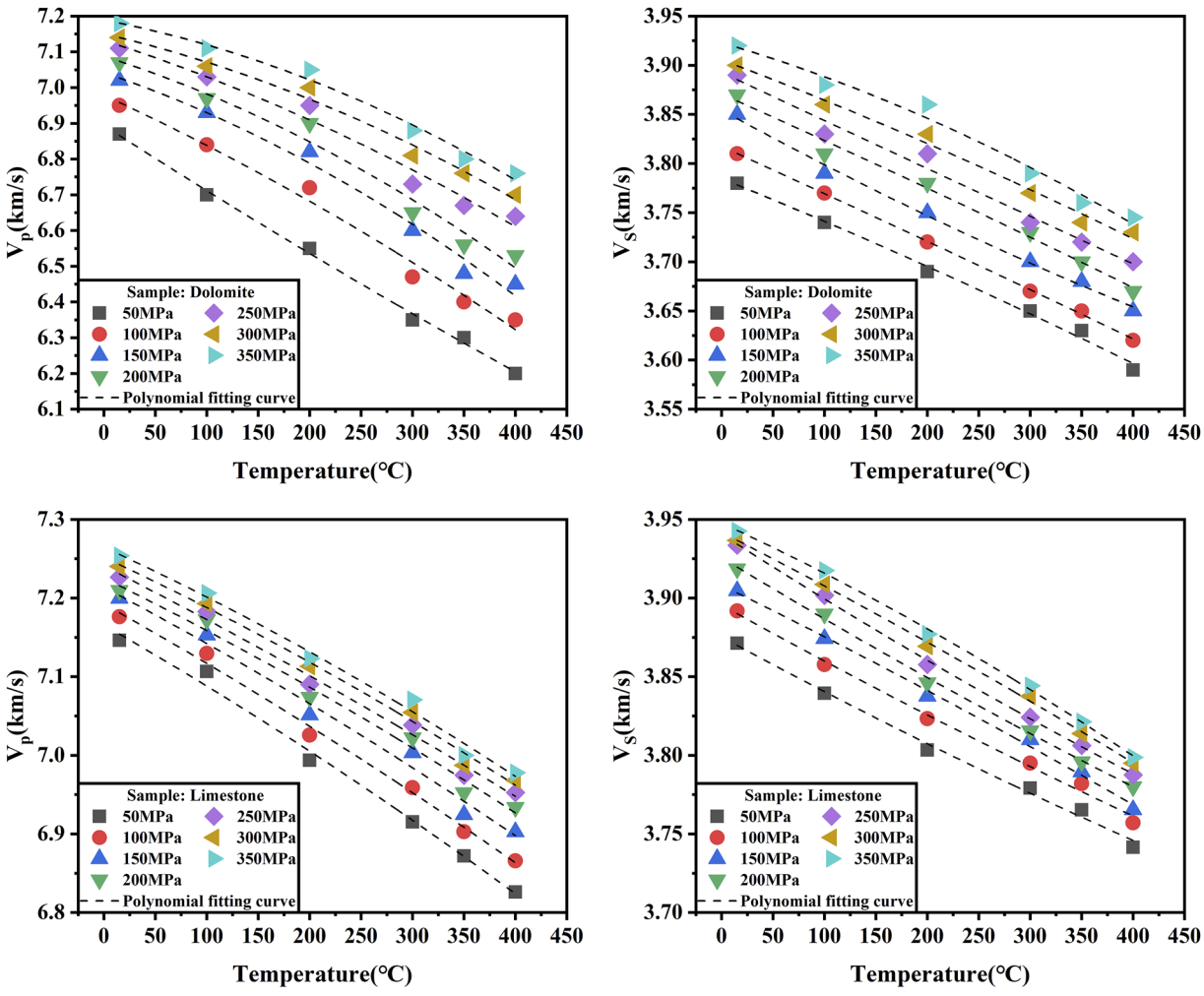

FIG. 9. The relationship between V_P and V_S of dolomite and limestone with temperature.

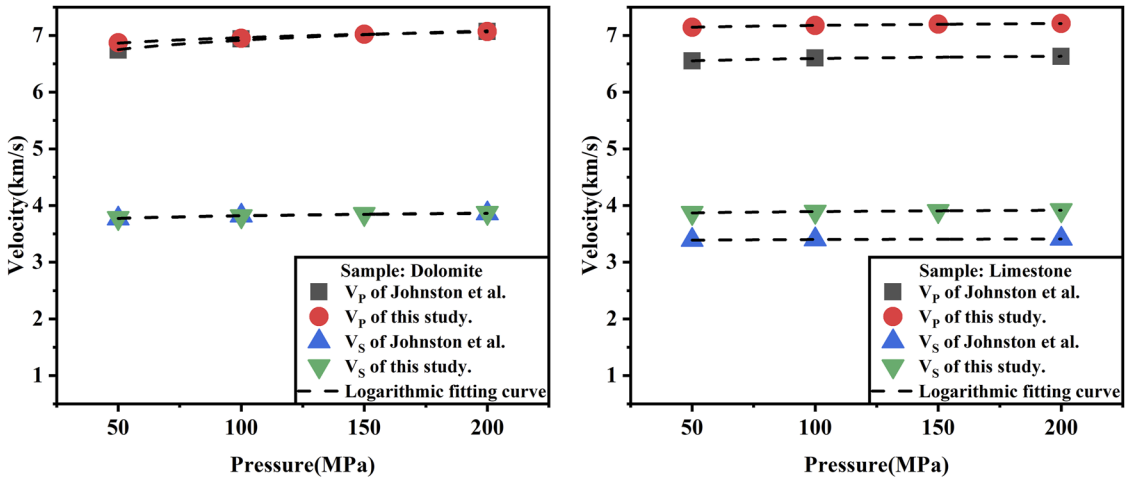

FIG. 10. Comparison of the experimental data in this paper with Johnston *et al.*'s experimental data.

dolomite increase with the increase in pressure. Specifically, around 200 MPa is a cut-off point. When the confining pressure is less than 200 MPa, the V_P and V_S of limestone and dolomite increase rapidly. When the pressure is greater than 200 MPa, because of the massive closure of the rock pores and fractures, the V_P and V_S of limestone and dolomite increase relatively slowly with the pressure. The variation trend in the elastic wave velocity of limestone and dolomite is consistent with the previous research results.[51–54]

2. The effect of temperature on the elastic wave velocity of limestone and dolomite

The experimental results of the effect by temperature on the elastic wave velocity of limestone and dolomite are shown in Fig. 9. When the confining pressure is constant, both the V_P and V_S of the limestone and dolomite decrease with the increase in temperature. V_P and V_S decrease approximately linearly with the increase in temperature, which is mainly related to the reduction in rock bulk modulus and the expansion of pores and fissures in the rock due to the increase in temperature.[55]

Finally, the experimental results in this paper are compared with the elastic wave velocity of limestone and dolomite measured by Johnston *et al.*[56] at room temperature and high pressure. It can be seen in Fig. 10 that although the differences in density, mineral composition, and pore structure of individual rocks result in different elastic wave velocities, the changing trends of the two elastic wave velocities are very similar. The feasibility of the equipment is verified to a certain extent by this comparison.

IV. POTENTIAL APPLICATION

In the practical geophysical exploration, the elastic wave velocity of rocks is usually measured under low-frequency seismic wave conditions (10–100 Hz), while in the laboratory, the elastic wave velocity of rocks is usually measured under high-frequency ultrasonic waves conditions (MHz level).[57] According to the results of previous studies,[57] it is known that the elastic wave velocity of rocks is a function of frequency and will vary with frequency, namely, frequency dispersion. Therefore, due to the presence of frequency dispersion, the elastic wave velocity of rocks measured under high-frequency conditions in the laboratory cannot be directly used in practical geophysical exploration, but usually needs to be processed as follows. Currently, in order to use the elastic wave velocity of rocks measured under high-frequency conditions in the laboratory for practical geological exploration, it is generally assumed that dry rock has no dispersion or negligible dispersion.[57,58] That is, the elastic wave velocity of rocks measured at high-frequency conditions in the laboratory is approximately equal to the elastic wave velocity of rocks at low-frequencies conditions. Then, the desired elastic wave velocity of rocks containing fluid at low frequencies can be obtained by adding the effect of fluid through the Gassmann theory.[59] Then, by comparing the elastic wave velocity of rocks after the above processing with the seismic wave velocity distribution obtained in seismic exploration, it is possible to infer the reservoir structure and constrain the uncertainty of geophysical inversion to some extent.[8,9]

V. CONCLUSION

Based on the importance of the rock elastic wave velocity in ultra-deep reservoir exploration, various devices for measuring the elastic wave velocity of rocks have been developed in the past, but the choice of equipment that can measure the elastic wave velocity of rocks under conditions of ultra-deep reservoirs deeper than 8 km is seriously insufficient. Then, we have developed this measurement equipment for the elastic wave velocity of rocks under temperature and pressure conditions of ultra-deep reservoirs. This equipment was capable of measuring the elastic wave velocity of rocks under temperature and pressure conditions of reservoirs up to a depth of 13 km. The feasibility of the equipment was verified

by comparing the elastic wave velocities of dolomite and limestone with the previous results reported in the literature. The equipment can be a useful addition to the current equipment for measuring the elastic wave velocity of rocks. The elastic wave velocity obtained by this equipment could potentially be applied in ultra-deep reservoir exploration. Nevertheless, our experimental equipment still needs to be improved, such as by making it capable of loading pore fluid pressure to better simulate the conditions of ultra-deep reservoirs.

ACKNOWLEDGMENTS

This work was financially supported by the National Natural Science Foundation of China (Grant No. 41873075) and the Major State Research Development Program of China (Grant No. 2016YFC0601101).

AUTHOR DECLARATIONS

Conflict of Interest

The authors have no conflicts to disclose.

Author Contributions

Shuai Wang: Data curation (equal); Investigation (equal); Methodology (equal). **Heping Li**: Data curation (equal); Funding acquisition (equal); Investigation (equal); Methodology (equal); Project administration (equal); Resources (equal); Supervision (equal); Validation (equal). **Yonggang Liu**: Funding acquisition (equal); Methodology (equal); Resources (equal). **Shengbin Li**: Methodology (equal). **Shuangming Shan**: Resources (equal). **Sen Lin**: Methodology (equal).

DATA AVAILABILITY

The data that support this study are available from the corresponding author upon reasonable request.

REFERENCES

[1] A. I. Best, Geophys. Prospect. **45**(2), 345–364 (1997).
[2] L. E. A. Jones and H. F. Wang, Geophysics **46**(3), 288–297 (1981).
[3] M. N. Toksöz, C. H. Cheng, and A. Timur, Geophysics **41**(4), 621–645 (1976).
[4] Y. Shen, X. Lü, S. Guo, X. Song, and J. Zhao, J. Nat. Gas Sci. Eng. **46**, 119–131 (2017).
[5] Z. Wang, Geophysics **66**(2), 398–412 (2001).
[6] M. S. King, Int. J. Rock Mech. Min. Sci. **46**(8), 1341–1348 (2009).
[7] Y. Liu, H. Xie, J. Guo, W. Zhou, J. Xu, and Z. Zhao, Chin. Phys. Lett. **17**(12), 924–926 (2000). https://www.doi.org/10.1088/0256-307X/17/12/024.
[8] B. A. Luke, C. Calderón-Macías, R. C. Stone, and M. Huynh, in *16th EEGS Symposium on the Application of Geophysics to Engineering and Environmental Problems* (EAGE, 2003), p. cp-190.
[9] R. G. Ellis and D. W. Oldenburg, Geophys. J. Int. **116**(1), 5–11 (1994).
[10] L. Vernik, J. Castagna, and S. J. Omovie, Geophysics **83**(1), MR35–MR45 (2017).
[11] S. Sharma, S. Thakur, and T. Sharma, IOP Conf. Ser.: Earth Environ. Sci. **889**(1), 012015 (2021).
[12] D. Sadeq, K. Alef, S. Iglauer, M. Lebedev, and A. Barifcani, Int. J. Hydrogen Energy **43**(52), 23193–23200 (2018).
[13] T. Liu, X. Liu, and T. Zhu, Mar. Pet. Geol. **112**, 104036 (2020).
[14] H. Bureau and M. Burchard, High Pressure Res. **26**(3), 233–234 (2006).
[15] E. Spangenberg, K. Seyberth, K. U. Heeschen, M. Priegnitz, and J. M. Schicks, J. Geophys. Res.: Solid Earth **123**(7), 5588–5598, https://doi.org/10.1029/2018jb015855 (2018).
[16] B. Li and R. C. Liebermann, Proc. Natl. Acad. Sci. U. S. A. **104**(22), 9145–9150 (2007).
[17] B. Li, I. Jackson, T. Gasparik, and R. C. Liebermann, Phys. Earth Planet. Inter. **98**(1-2), 79–91 (1996).
[18] B. Li, J. Kung, T. Uchida, and Y. Wang, J. Appl. Phys. **98**(1), 013521 (2005).
[19] F. Decremps, L. Belliard, B. Perrin, and M. Gauthier, Phys. Rev. Lett. **100**(3), 035502 (2008).
[20] H. J. Mueller, J. Lauterjung, F. R. Schilling, C. Lathe, and G. Nover, Eur. J. Mineral. **14**(3), 581–589 (2002).
[21] J. Du, Y. Li, C. Wang, and L. Liu, *High Pressure Geoscience* (Seismological Press, Beijing, 2010), pp. 21–22 (In Chinese).
[22] S. Shan, C. Xiao, H. Li, L. Xu, S. Lin, and S. Li, Rev. Sci. Instrum. **92**(9), 095104 (2021).
[23] K. Kitamura, K. Masuda, M. Takahashi, and O. Nishizawa, Earth, Planets Space **58**(11), 1515–1518 (2006).
[24] T. Watanabe and A. Higuchi, Geofluids **14**(3), 372–378 (2013).
[25] A. Zappone, M. Fernàndez, V. García-Dueñas, and L. Burlini, Tectonophysics **317**(3-4), 259–272 (2000).
[26] H. Li, D.-h. Han, M. Sun, H. Yuan, and J. Gao, Energy **238**, 122011 (2022).
[27] Rock Mechanics Test Systems, MTS Systems Corporation, https://www.mts.com/en/products/rock-geomechanics/rock-mechanics-test-systems.
[28] High Temperature AutoLab, New England Research, Inc., http://www.ner.com/site/systems/autolab-series/high-temp-autolab.html.
[29] Rock Triaxial Testing Systems, GCTS Testing Systems, https://www.gcts.com/product/rock-triaxial-test/.
[30] High-Pressure High-Temperature Triaxial System, Wille Geotechnik, https://www.wille-geotechnik.com/en/high-pressure-high-temperature-triaxial-system-hp-ht.html.
[31] U. Arslan and D. Huber, 3rd, in International Conference on New Developments in Soil Mechanics and Geotechnical Engineering, Nicosia, North Cyprus, 2012, pp. 723–730.
[32] L. Tajmanová, J. Metamorph. Geol. **33**(8), 783–784 (2015). https://www.doi.org/10.1111/jmg.12152.
[33] D. L. Anderson, "The Crust and Upper Mantle," in *Theory of the Earth* (Blackwell Scientific, Boston, MA, 1989), pp. 45–47 http://resolver.caltech.edu/CaltechBOOK:1989.001.
[34] C. R. Krüger and E. G. Rochow, J. Polym. Sci. **2**(7), 3179–3189 (1964).
[35] T. Watanabe, H. Kasami, and S. Ohshima, Earth, Planets Space **59**(4), 233–244 (2007).
[36] M. Ramezanian and H. Emadi, Geomech. Energy Environ. **22**, 100179 (2020).
[37] S. Stanchits, S. Vinciguerra, and G. Dresen, Pure Appl. Geophys. **163**(5-6), 975–994 (2006).
[38] L. Sun, C. Zou, R. Zhu, Y. Zhang, S. Zhang, B. Zhang, G. Zhu, and Z. Gao, Pet. Explor. Dev. **40**(6), 687–695 (2013).
[39] X. Guo, D. Hu, Y. Li, J. Duan, and W. Li, Engineering **5**(3), 458–470 (2019).
[40] G. Zhu, A. V. Milkov, J. Li, N. Xue, and Z. Chen, J. Pet. Sci. Eng. **199**(4), 108246 (2020).
[41] Z. He, Y. Ma, D. Zhu, T. Duan, J. Geng, J. Zhang, Q. Ding, Y. Qian, Y. Wo, and Z. Gao, Oil Gas Geol. **42**(3), 533–546 (2021) (In Chinese).
[42] L. Liu, H. Li, H. Zhou, S. Lin, and S. Li, Minerals **12**(2), 127 (2022).
[43] S. Li, H. Li, S. Lin, S. Shan and L. Liu, CN patent No. CN 109669074A (23 April 2019).
[44] H. Li, L. Zhou, L. Xu, M. Yang and H. Xu, CN patent No. CN203469947U (12 March 2014).

[45]A. Voleišis, R. Kažys, B. Voleišienė, and R. Sliteris, Ultragarsas/Ultrasound **66**(1), 25–31 (2011). https://www.doi.org/10.5755/j01.u.66.1.263.
[46]R. Kazys and V. Vaskeliene, Sensors **21**(9), 3200 (2021).
[47]S. Ha, K. Lonkar, A. Mittal, and F.-K. Chang, Struct. Health Monit. **9**(3), 247–256 (2010).
[48]R. Bansal, Appl. Microwave Wireless **11**(11), 59–60 (1999).
[49]Y. Liu, H. Xie, W. Zhou, and J. Guo, J. Phys.: Condens. Matter **14**(44), 011381 (2002).
[50]X. H. Zhang, Z. G. Qu, D. Tian, and Y. Fang, Appl. Acoust. **151**, 22–29 (2019).
[51]D. S. Hughes and C. Maurette, Geophysics **22**(1), 23–31 (1957).
[52]F. Birch, J. Geophys. Res. **65**(4), 1083–1102, https://doi.org/10.1029/jz065i004p01083 (1960).
[53]F. Birch, J. Geophys. Res. **66**(7), 2199–2224, https://doi.org/10.1029/jz066i007p02199 (1961).
[54]N. I. Christensen, J. Geophys. Res. **84**(BI2), 6849–6857, https://doi.org/10.1029/jb084ib12p06849 (1979).
[55]H. Kern, Tectonophysics **44**(1-4), 185–203 (1978).
[56]J. E. Johnston and N. I. Christensen, Tectonophysics **210**(1-2), 1–20 (1992).
[57]K. W. Winkler, Geophysics **51**(1), 183–189 (1986).
[58]G. A. Gist, Geophysics **59**(7), 1100–1109 (1994).
[59]M. S. King and J. R. Marsden, Geophysics **67**(1), 254–258 (2002).